JOURNAL OF MATERIALS SCIENCE **34** (1999) 4193–4197

Study on the effects of Cr_2O_3 on the reduction behavior of γ-Fe_2O_3

L. S. CHEN, G. L. LÜ
Central Lab. Zhejiang University, Hangzhou 310028, People's Republic of China
E-mail: gllu.@tiger.hzuniv.edu.cu

XRD and TG reduction analysis show that γ-Fe_2O_3 Fe-Cr catalysts, which contains 0.0 to 14.0 wt%. Cr_2O_3 and prepared by coprecipitating method, consist of crystalline γ-Fe_2O_3 and non-crystalline Fe_2O_3. Between 150–450 °C, three reduction stages are observed in the catalyst. The first stage is non-crystalline Fe_2O_3 reduced to non-crystalline Fe_3O_4, the second is crystalline γ-Fe_2O_3 to crystalline Fe_3O_4 and the third is non-crystalline Fe_2O_3 reduced to non-crystalline FeO. About 5 wt%. Cr_2O_3 can enter the lattices of γ-Fe_2O_3 to form solid solution. With the increasing of Cr_2O_3 content, the relative abundance of non-crystalline Fe_2O_3 and the amount of soluble Cr_2O_3 in non-crystalline increases, while the crystalline size of γ-Fe_2O_3 decreases. © *1999 Kluwer Academic Publishers*

1. Introduction

The iron oxide/chromium oxide catalysts are widely used industrially. Usually, Cr_2O_3 is introduced into Fe_2O_3 by coprecipitating method or mixture method. Before use, Fe_2O_3 must be reduced to Fe_3O_4 which is thought to be the active component of the iron oxide/chromium oxide catalyst. It is generally believed that Cr_2O_3 acts as a stabilizer rather than a promoter, and prevents high temperature sintering and loss of surface area of Fe_3O_4 [1]. There are few reports, however, on Cr_2O_3 existing states and its effects on Fe_2O_3 reduction behavior.

Our previous papers [2–4] shown that Fe_3O_4, obtained from γ-Fe_2O_3 prepared by coprecipitating method using $Fe^{3+}(Cr^{3+})/Fe^{2+}$ mixture, had better low temperature catalytic activities than Fe_3O_4 obtained from α-Fe_2O_3 prepared by using $Fe^{3+}(Cr^{3+})$ mixture. The difference of activity is contributed to the different bulk and microstructures in these Fe_3O_4. We also found that the reduction behavior and catalytic activity of Fe_3O_4 obtained from γ-Fe_2O_3 depended on the concentration of Cr_2O_3 additive. It is important to elucidate the influence of the concentration of Cr_2O_3 additive on the structure of the catalysts. In this paper, we use XRD Rietveld analysis and TG reduction experiments to study the effects of the concentration of Cr_2O_3 additive on the structure and reduction behavior of the catalysts.

2. Experimental

2.1. Sample preparation

Samples were prepared by $Fe^{3+}(Cr^{3+})/Fe^{2+}$ mixture coprecipitating method [2]. A solution of an AR grade $FeSO_4$, $Fe_2(SO_4)_3$ containing $Cr_2(SO_4)_3$ coprecipitated with ammonia at pH = 8 and 60 °C. The suspensions were filtered and washed carefully with distilled water until all SO_4^{2-} was eliminated. Then the precipitates were dried at 120–160 °C and calcined at 350 °C for 3 h in air atmosphere.

2.2. TG and DTG

TG and DTG apparatus employed was a Delta Series TGA7 (Perkin-Elmer Co.), and operated under the following conditions: the reduction gas was a mixture of 5% H_2 and 95% N_2 (v/v) with a flow rate of 50 ml min^{-1}. The heating rate was 10 °C min^{-1}, and the temperature range was 150–450 °C. Before the experiment, the sample was heated at 200 °C in N_2 atmosphere until no mass loss, then cooled down to 150 °C, and subsequently the reduction gas was introduced to start the reduction.

Each peak site in DTG curves corresponding to one reaction process. For overlapping reactions, the minimum in the DTG curve is used to define the end of the first mass-loss and the onset of the second [5]. Balance sensitivity is 10^{-4} mg and its accuracy better than 0.1%. The accuracy of temperature is ±3 °C.

2.3. H_2-TPR

Samples of catalysts (5–10 mg) were placed in a quartz tubular reactor (ϕ = 6 mm) which connected to a conventional TPR apparatus. The reduction gas contained 5% H_2 in N_2 with a total flow of 50 ml min^{-1}, and its heating rate was 10 °C min^{-1}. The reduction gas was purified by Pd/Al_2O_3 and 5 Å molecular sieve before being introduced into reactor.

Hydrogen uptakes and evolutions were estimated by integration of the TPR signal, the detector response being calibrated by injection doses of pure hydrogen.

2.4. XRD

XRD data were collected with Rigaku D/max-3B X-ray powder diffractometer, using CuK_α radiation and a

diffracting beam monochrometer under the power of 40 kV × 30 mA.

The amorphous content and cell parameters of the samples were determined by multiphase Rietveld analysis using DBWS9006 program package [6]. The internal standard was α-Fe_2O_3 of AR grade after calcined at 900 °C for 5 h. The ratio of sample to α-Fe_2O_3 was 1. Using the Rietveld scale factor S_α and S_r of α-Fe_2O_3 and γ-Fe_2O_3, the amorphous could be obtained from the following equation [7]:

$$W_{r\alpha} = 1 - [W_\alpha S_r(ZMV)_r / S_\alpha(ZMV)_\alpha]/W_s$$

where $W_{r\alpha}$ is the amorphous abundance of γ-Fe_2O_3, W_α is the relative weight fraction of α-Fe_2O_3 in the mixture of internal standard and sample, W_s is the relative weight fraction of sample in the mixture, and Z, M and V are the number of formula units per unit cell, the mass of formula unit (in atomic mass units) and the unit cell volume (in Å^3), respectively. The crystallite size of sample's 440 diffraction was determined by voigt function single-line analysis method [8]. The instrumental broadening was obtained by using the profiles of BaF_2 calcined at 500 °C for 5 h [9].

3. Results and discussion

3.1. Thermal analysis

Figs 1 and 2 show TG and DTG curves of samples containing 0, 4, 8, and 12 wt%. Cr_2O_3 respectively. According to the TG and DTG curves, three reduction stages can be observed in all samples.

Table I lists the weight loss of samples in each reduction stage and their O/Fe atom ratios after deducting Cr_2O_3 additive (Cr_2O_3 is not reduced before 450 °C [10]). The O/Fe atom ratios of samples in three reduction stages are 1.476 to 1.454, 1.333 to 1.301 and 1.297 to 1.193 respectively. Comparing to 1.5, 1.333, 1.0 of γ-Fe_2O_3, Fe_3O_4 and FeO respectively, the first stage is between γ-Fe_2O_3 and Fe_3O_4, and partial Fe_2O_3 was reduced to Fe_3O_4. The second stage corresponds to all Fe_2O_3 reduced to Fe_3O_4, and FeO was detected in samples which overtake 4 wt% Cr_2O_3. In the third stage, partial Fe_3O_4 was reduced to FeO.

TABLE I Weight loss and O/Fe atom ratio of Fe-Cr water-gas shift catalysts in each reduction stage

	Stage I		Stage II		Stage III	
Cr_2O_3 content of sample (%)	Weight loss (%)	O/Fe atom ratio	Weight loss (%)	O/Fe atom ratio	Weight loss (%)	O/Fe atom ratio
0	0.48	1.476	2.87	1.333	0.71	1.297
2	0.47	1.476	2.80	1.332	1.08	1.278
4	0.53	1.472	2.77	1.325	1.33	1.259
6	0.62	1.467	2.74	1.317	1.65	1.235
8	0.72	1.461	2.67	1.311	1.82	1.221
10	0.82	1.454	2.68	1.301	2.16	1.193
12	0.96	1.445	2.66	1.290	2.53	1.162
14	1.08	1.437	2.52	1.286	3.96	1.090

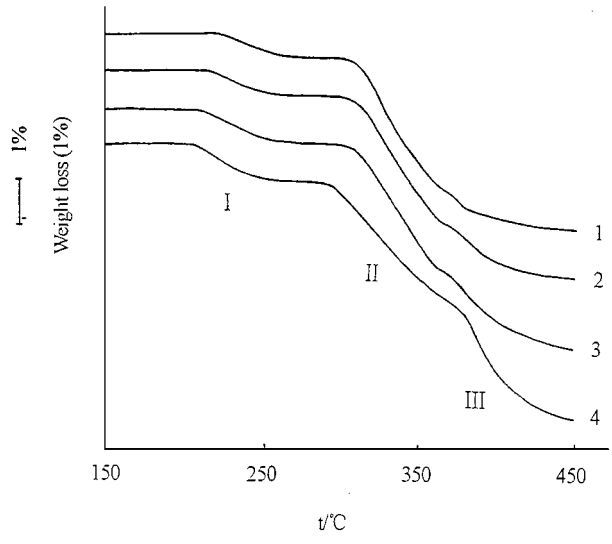

Figure 1 TG profiles of Fe-Cr water-gas shift catalysts: (1) 0 wt% Cr_2O_3; (2) 4 wt% Cr_2O_3; (3) 8 wt% Cr_2O_3; and (4) 12 wt% Cr_2O_3. I, II, and III are three reduction stages.

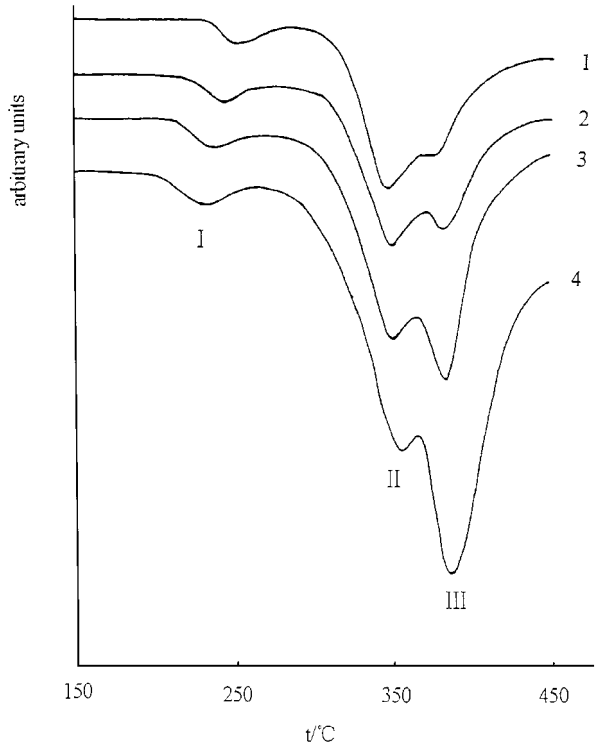

Figure 2 DTG profiles of Fe-Cr water-gas shift catalysts: (1) 0 wt% Cr_2O_3; (2) 4 wt% Cr_2O_3; (3) 8 wt% Cr_2O_3; and (4) 12 wt% Cr_2O_3. I, II, and III are three reduction stages.

3.2. Temperature-programmed reduction

Fig. 3 is a TPR curves of 8 wt% Cr_2O_3 and 12 wt% Cr_2O_3 two Fe-Cr water-gas shift catalysts. Table II lists the peak temperatures of TPR and amount of H_2 consumption. It is thought that the reduction of Fe_2O_3 proceeds stepwise through reaction (1) and (2). According to Table II, the reduction reaction contains three stages, and we can calculate the percentage of reduced Fe_2O_3 in the first and second stages through reaction (1).

$$3Fe_2O_3 + H_2 \rightarrow 2Fe_3O_4 + H_2O \quad (1)$$

$$Fe_3O_4 + H_2 \rightarrow 3FeO + H_2O \quad (2)$$

TABLE II H_2 consumption amount (mmol $H_2 \cdot mg^{-1}$ sample) and peak temperatures of two water-gas shift catalysts in three reduction stages

	Stage I		Stage II		Stage III	
Cr_2O_3 content of samples (%)	H_2 consumption (10^{-3} mmol)	t (°C)	H_2 consumption (10^{-3} mmol)	t (°C)	H_2 consumption (10^{-3} mmol)	t (°C)
8	0.478	246	1.381	310	0.901	331
12	0.728	241	1.131	317	1.449	340

For 8 wt % Cr_2O_3 sample, 23.0% Fe_2O_3 was reduced in I and 66.3% in II, for 12 wt % Cr_2O_3 sample, 34.9% in I and 54.3% in II. About 90% Fe_2O_3 was reduced in I and II. So the third stage proceeds through reaction (2) while H_2 uptake of the third stage is twice as much as that of the first stage.

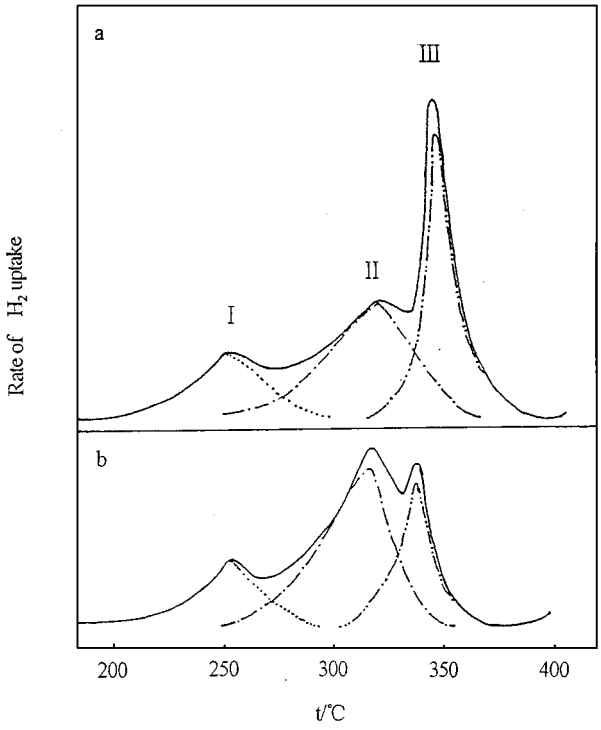

Figure 3 TPR curves of two Fe-Cr water-gas shift catalysts (a) 12 wt % Cr_2O_3 and (b) 8 wt % Cr_2O_3. I, II, and III are three reduction stages.

3.3. XRD results

Fig. 4 shows the XRD patterns of samples with various Cr_2O_3 content. From Fig. 4, the crystalline phase of all samples are γ-Fe_2O_3. Fig. 5 shows the XRD patterns of 14 wt % Cr_2O_3 that obtained from different reduction stages and preserved with Ar and benzene from oxiding. It is obviously shown that XRD patterns of the first stage are analogy to that of unreduced sample. The second and the third stages are also analogy, but the diffraction peaks shift to low angles. And d value of 2.03 Å of α-Fe could be detected in the third stage. The crystalline phase of iron-oxide is γ-Fe_2O_3 in the first stage, while it is Fe_3O_4 phase which has the same structural type but smaller cell parameters than γ-Fe_2O_3 in the second and the third stages. Non other crystallie oxides were detected except γ-Fe_2O_3 and Fe_3O_4 in three reduction stages.

Fig. 6 shows the Rietveld analysis profile of 14 wt % Cr_2O_3 sample. Table III lists the abundance of amorphous, cell parameters of γ-Fe_2O_3 and crystallite size of 440 tendency of different Cr_2O_3 content samples obtained from Rietveld analysis. It can be found that the change direction of the abundance of amorphous, cell parameters and crystallite size of γ-Fe_2O_3 have a good correspondence to the additive quantitative of Cr_2O_3. The cell parameters decreased with the increasing of Cr_2O_3 content, the ionic radius of Cr^{3+} and Fe^{3+}

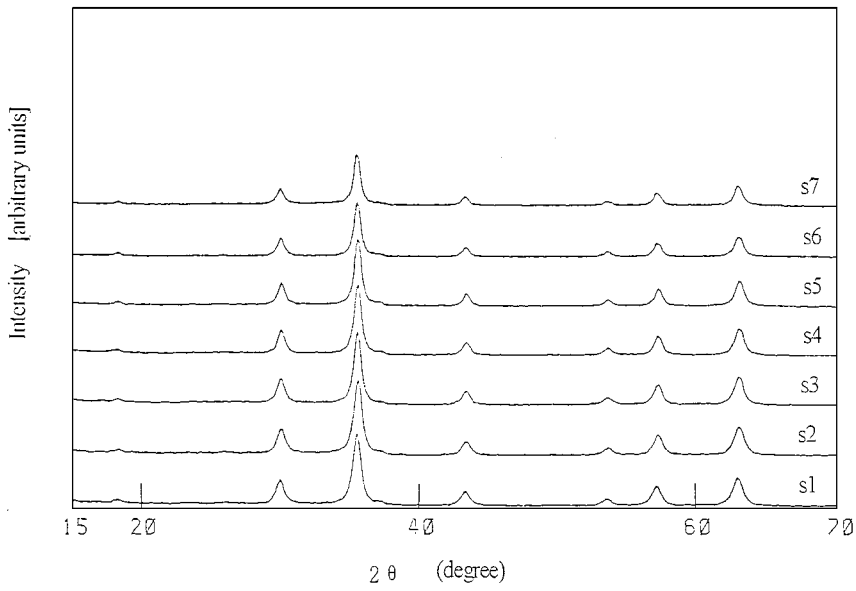

Figure 4 XRD profiles of Fe-Cr water-gas shift catalysts. S1: 0 wt % Cr_2O_3, S2: 2 wt % Cr_2O_3, S3: 4 wt % Cr_2O_3, S4: 6 wt % Cr_2O_3, S5: 8 wt % Cr_2O_3, S6: 10 wt % Cr_2O_3, and S7: 12 wt % Cr_2O_3.

TABLE III The amorphous abundance, cell parameters and 440 direction crystallite size of catalysts with different content of Cr_2O_3

Cr_2O_3 content of sample (%)	Amorphous abundance (%)	Cell parameter (nm)	Crystallite size of 440 direction (nm)
0	21.74	0.83442	24.5
2	21.73	0.83401	23.1
4	22.10	0.83394	20.6
6	25.50	0.83389	20.4
8	28.50	0.83390	20.5
10	35.48	0.83391	20.4
12	41.82	0.83383	16.1
14	48.60	0.83387	15.2

are 0.64 and 0.67 Å respectively, and the solid soluble Cr_2O_3 in crystalline γ-Fe_2O_3 kept stable when the content of Cr_2O_3 surpassed 4 wt %, so that the largest additive quantitative of Cr_2O_3 in crystalline γ-Fe_2O_3 did not surpass 5 wt %.

3.4. Structure analysis of three reduction stages

TG and TPR show that reduction of all samples had three stages which related to the three structure states between 150–450 °C. From Fig. 5, Table I, Table III, we can found that crystalline γ-Fe_2O_3 did not be reduced

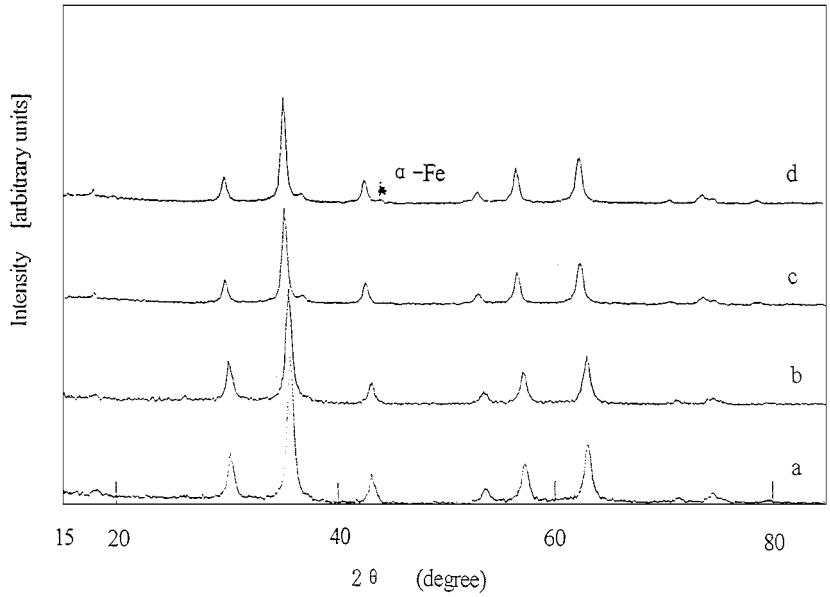

Figure 5 XRD profiles of three reduction stages for 14 wt % Cr_2O_3 sample: (a) 14 wt % Cr_2O_3 sample; (b) I stage's sample; (c) II stage's sample; and (d) III stage's sample.

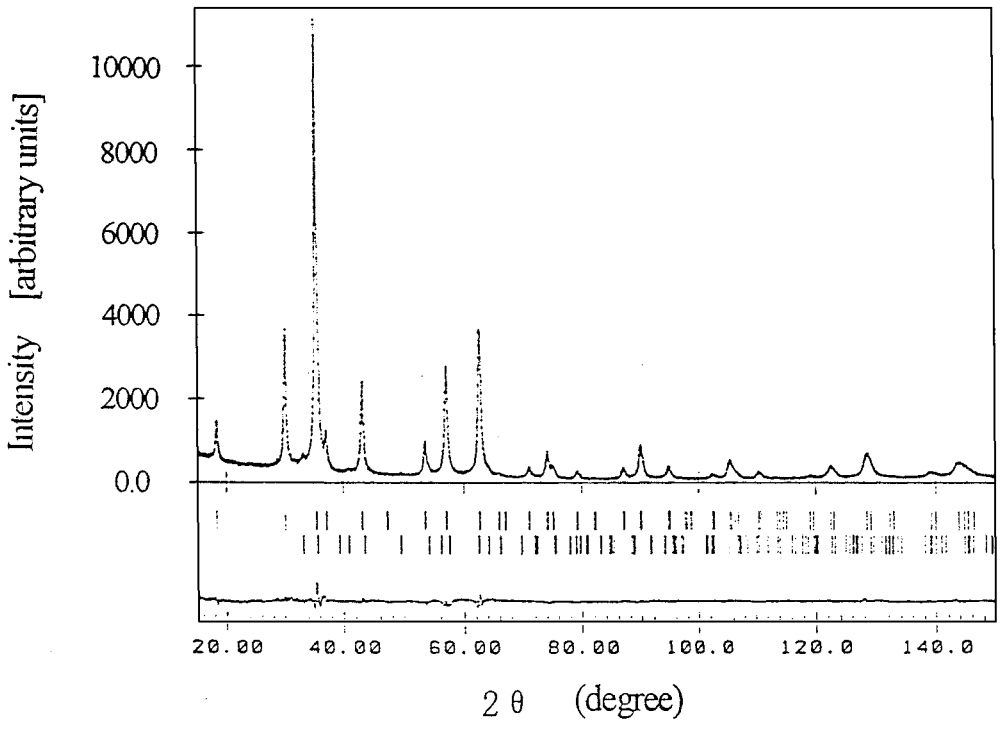

Figure 6 Rietveld analysis profile of 14 wt % Cr_2O_3: Dotline—the observed pattern; Continuous line—the calculated pattern; and Lower curves—the difference between the observed and calculated pattern. The rows of tick marks from up to down are the position of all possible Bragg reflections of γ-Fe_2O_3 and α-Fe_2O_3 respectively.

TABLE IV The percent content of γ-Fe_2O_3, Fe_3O_4 and FeO of Fe-Cr water-gas shift catalysts in each reduction stage and their XRD amorphous abundance

Cr_2O_3 content of samples (%)	Stage I		Stage II		Stage III		XRD amorphous abundance of Fe_2O_3 (%)
	γ-Fe_2O_3 (%)	Fe_3O_4 (%)	Fe_3O_4 (%)	FeO (%)	Fe_3O_4 (%)	FeO (%)	
0	85.6	14.4	100	0	89.1	10.9	21.7
2	85.6	14.4	99.6	0.4	83.4	16.6	21.7
4	83.2	16.8	97.5	2.5	77.7	22.3	22.1
6	80.2	19.8	95.1	4.9	70.5	29.5	25.5
8	76.6	23.4	93.3	6.7	66.3	33.7	28.5
10	72.4	27.6	90.3	9.7	57.9	42.1	35.5
12	67.0	33.0	87.0	13.0	48.6	51.4	41.8
14	62.2	37.8	85.8	14.2	27.0	73.0	48.6

in the first stage, the atom ratio of O/Fe was less than 1.5 of Fe_2O_3 and bigger than 1.333 of Fe_3O_4, but γ-Fe_2O_3 had changed to crystalline Fe_3O_4 in the second stage, the atom ratio of O/Fe was near 1.333 of Fe_3O_4. So that amorphous Fe_2O_3 reduced to amorphous Fe_3O_4, amorphous Fe_3O_4 and crystalline γ-Fe_2O_3 coexisted in the first stage. In the second stage, crystalline γ-Fe_2O_3 reduced to crystalline Fe_3O_4, crystalline Fe_3O_4 and amorphous Fe_2O_3 coexisted. In the third stage, the atom ratio of O/Fe was bigger than 1.0 of FeO, but less than 1.333 and crystalline Fe_3O_4 was not reduced, but amorphous Fe_3O_4 was reduced to amorphous FeO, so amorphous FeO and crystalline Fe_3O_4 coexisted. All kinds of amorphous Fe_2O_3 could not be detected by XRD, but TG, O/Fe atom ratio and TPR tested them existing and having different TG reduction behaviors with crystalline γ-Fe_2O_3. In our experiments, crystallite Fe_3O_4 was directly reduced to α-Fe not to crystallite FeO.

3.5. The effects of Cr_2O_3 content on the structure and reduction behaviors of γ-Fe_2O_3

Table IV lists the percentage of amorphous Fe_3O_4 in the first stage, amorphous FeO in the second and third stages deduced from TG weight loss, and the abundance of amorphous Fe_2O_3 in fresh samples obtained from XRD Rietveld analysis. The amorphous abundance in different reduction stages had the same tendency though their amorphous abundance was not completely similar. It showed that the abundance of amorphous Fe_2O_3 increased with the increasing of Cr_2O_3 content. The abundance obtained from XRD Rietveld analysis is bigger than that from TG and TPR. This is because XRD results counted on crystallite. It did not include the non-crystalline layer around every crystal grain [11]. In other words, there are structural layers that have less stable than crystallite but little more stable than non-crystallite on the surface of crystallite salts and oxides [12]. And the amorphous calculated from TG and TPR did not include these, so that the abundance was less than that of XRD results. From the change of FeO content deduced from Fe/O ratio of the second stage, the amorphous Fe_3O_4 began to transform amorphous FeO with the increasing of Cr_2O_3. The reduction temperature of changing to α-Fe also lowered with the increasing of Cr_2O_3 content. According to the change of cell parameters and crystallite size of γ-Fe_2O_3 in Table III, it can be found that cell parameters kept stable and crystallite size got smaller when the concentration of Cr_2O_3 surpassed 4 wt%. In addition, the decreasing of initial reduction temperature resulted from the crystallite size getting smaller. The same results were also reported in α-Fe_2O_3 reduction [10].

Conclusion

1. For Fe-Cr water-gas shift catalyst prepared by co-precipitate method, the amorphous content increased with the increasing of Cr_2O_3. When it was reduced between 150–450 °C, the catalyst has three reduction stages. They are amorphous Fe_2O_3 reduced to amorphous Fe_3O_4, crystalline γ-Fe_2O_3 reduced to crystalline Fe_3O_4, and amorphous Fe_3O_4 reduced to amorphous FeO.
2. About 5 wt% Cr_2O_3 can enter the lattices of γ-Fe_2O_3 to form solid solution. There are different weight contrast of Cr_2O_3/Fe_2O_3 in amorphous Fe_2O_3 and crystalline γ-Fe_2O_3.

Acknowledgement

This work was supported by Zhejiang Provincial National Science Foundation of China (NO292027).

References

1. M. I. MARKINA, G. K. BORESKOV, F. P. IVANOVSKII and B. G. LYUDKOVSHAYA, *Kinet* **2** (1961) 867.
2. L. S. CHEN, G. L. LÜ, R. G. LING, C. Z. XIE, X. Q. WANG and X. Y. ZHOU, *Chinese J. of Cat.* **15** (1994) 13.
3. L. S. CHEN and G. L. LÜ, *Acta Chimica Sinica* **53** (1995) 966.
4. G. L. LÜ, L. S. CHEN, S. H. LIU, Y. S. XU and S. XU, *ibid.* **54** (1996) 833.
5. WESLEY WM. WENDLANDT, "Thermal Analysis," 3rd ed., (Wiley-Interscience, 1986) p. 55.
6. D. B. WILES and R. A. YOUNG, *J. Appl. Cryst.* **14** (1981) 149.
7. R. J. HILL and C. J. HOWARD, *ibid.* **20** (1987) 467.
8. TH. H. DEKEIJSER, J. I. LANGFORD, E. J. MITTEMEIJER and A. P. B. VOGELS, *ibid.* **15** (1982) 308.
9. D. LOUER, J. I. LANGFORD, *ibid.* **21** (1988) 430.
10. M. SHIMOKAWABE, R. FURUICHI and T. ISHII, *Thermochimica Acta* **28** (1979) 287.
11. R. A. YOUNG, "The Rietveld Method" (Oxford Science Publication, 1993) p. 98.
12. Y. C. XIE, M. G. QIANG and Y. Q. TONG, *Chinese Sci. (B)* **9** (1983) 788.

Received 10 September 1998
and accepted 29 January 1999